Earliest land plants created modern levels of atmospheric oxygen

Timothy M. Lenton[1]*, Tais W. Dahl[2], Stuart J. Daines[1], Benjamin J. W. Mills[1,3], Kazumi Ozaki[4], Matthew R. Saltzman[5], Philipp Porada[6]

[1]Earth System Science, College of Life and Environmental Sciences, University of Exeter, Exeter EX4 4QE, UK.

[2]Natural History Museum of Denmark, Øster Voldgade 5-7, Copenhagen, Denmark.

[3]School of Earth and Environment, University of Leeds, Leeds LS2 9JT, UK.

[4]School of Earth and Atmospheric Sciences, Georgia Institute of Technology, 311 Ferst Drive, Atlanta, GA 30332-0340, USA.

[5]School of Earth Sciences, The Ohio State University, Columbus, Ohio 43214, USA.

[6] Department of Environmental Science and Analytical Chemistry, Stockholm University, Svante Arrhenius väg 8, SE-114 18 Stockholm, Sweden.

*Corresponding author:

Tim Lenton

Earth System Science, Laver Building (Level 7), North Park Road, University of Exeter, Exeter EX4 4QE, UK

Tel: +44 1392 724608

Email: t.m.lenton@exeter.ac.uk

ORC ID: 0000-0002-6725-7498

Classification: Physical Sciences; Earth, Atmospheric and Planetary Sciences

Short title: First plants oxygenated the atmosphere and ocean

Keywords: Oxygen, plants, phosphorus, weathering, Paleozoic

Abstract:

The progressive oxygenation of the Earth's atmosphere was pivotal to the evolution of life, but the puzzle of when and how atmospheric oxygen (O_2) first approached modern levels (~21%) remains unresolved. Redox proxy data indicate the deep oceans were oxygenated during 435-392 Ma, and the appearance of fossil charcoal indicates O_2 >15-17% by 420-400 Ma. However, existing models have failed to predict oxygenation at this time. Here we show that the earliest plants, which colonized the land surface from ~470 Ma onwards, were responsible for this mid-Paleozoic oxygenation event, through greatly increasing global organic carbon burial – the net long-term source of O_2. We use a trait-based ecophysiological model to predict that cryptogamic vegetation cover could have achieved ~30% of today's global terrestrial net primary productivity by ~445 Ma. Data from modern bryophytes suggests this plentiful early plant material had a much higher molar C:P ratio (~2000) than marine biomass (~100), such that a given weathering flux of phosphorus could support more organic carbon burial. Furthermore, recent experiments suggest that early plants selectively increased the flux of phosphorus (relative to alkalinity) weathered from rocks. Combining these effects in a model of long-term biogeochemical cycling, we reproduce a sustained +2‰ increase in the carbonate carbon isotope ($\delta^{13}C$) record by ~445 Ma, and predict a corresponding rise in O_2 to present levels by 420-400 Ma, consistent with geochemical data. This oxygen rise represents a permanent shift in regulatory regime to one where fire-mediated negative feedbacks on organic carbon burial stabilise high O_2 levels.

Significance statement:

The rise of atmospheric oxygen over Earth history has received much recent interdisciplinary attention. However, the puzzle of when and how atmospheric oxygen reached modern levels remains unresolved. Many recent studies have argued for a major oxygenation event – of uncertain cause – in the Neoproterozoic Era >541 million years ago (Ma), enabling the rise of animals. Previous modelling work has predicted a late Paleozoic oxygen rise (<380 Ma) due to the rise of forests. Here we show that neither scenario is correct. Instead the earliest plants, which colonized the land from 470 Ma onwards, first increased atmospheric oxygen to present levels by 400 Ma. This instigated fire-mediated feedbacks that have stabilised high oxygen levels ever since, shaping subsequent evolution.

\body

Introduction

After the well-defined 'Great Oxidation Event' 2.45-2.32 Ga, the trajectory of atmospheric oxygen is deeply uncertain (1, 2). Many recent studies, reviewed in (3-5), have argued for a Neoproterozoic oxygenation event (>550 Ma) – of uncertain cause – and have linked it to the rise of animals, but this has been questioned given a lack of change in iron-speciation ocean redox proxy data (6). Some models predict pO_2 ~1 PAL (present atmospheric level) already in the early Paleozoic (7, 8), but this is at odds with data for widespread ocean anoxia (6, 9). The 'COPSE' model we adapt here (10) predicts early Paleozoic pO_2 ~0.2-0.5 PAL consistent with redox proxy data, but like the other models (7, 8) it does not predict a rise in oxygen until the advent of forests starting ~385 Ma, and continuing until ~300 Ma. This is too late to explain marked changes in geochemical data that occur before ~390 Ma (figure 1). The first appearance of fossil charcoal in the late Silurian (11) and its ongoing occurrence through the Devonian (12) (table S1), albeit rare and at low concentrations, indicates O_2>15-17% (by volume) of the atmosphere (13) (or O_2>~0.7 PAL assuming a constant N_2 reservoir) already by ~420-400 Ma. (Under ideal conditions of ultra-dry fuel and forced airflow, smoldering fires may be sustained at O_2>10%, but this is not believed to be possible under natural conditions (14)). The molybdenum isotope record (9) indicates a fundamental shift in the redox state of the deep ocean from widespread anoxia to widespread oxygenation sometime during 435-392 Ma (between the early Silurian and the mid-Devonian). This ocean oxygenation is also supported by a Silurian increase in the C/S ratio of shales (15), and a shift in iron-speciation data sometime during 435-387 Ma (6).

The persistent oxygenation of the ocean and appearance of charcoal can be explained by a rise in atmospheric oxygen occurring by ~400 Ma. This could be due to a persistent increase in oxygen source – considered here – or a decrease in oxygen sink (16), leading to a reorganization of the Earth's surface redox balance at a higher steady-state level for atmospheric O_2. The major long-term source of oxygen to the atmosphere is the burial of organic carbon in sedimentary rocks (which represents the net flux of photosynthesis minus various pathways of respiration and oxidation). Increases in global organic carbon burial are recorded as positive shifts in the isotopic composition of carbonate rocks ($\delta^{13}C$). Consistent with a rise in oxygen, the carbon isotope record (17) (figure 1) indicates a fundamental shift in baseline from ≤0‰ prior to the Late Ordovician to ~2‰ from ~445 Ma onwards. Whilst there are many subsequent $\delta^{13}C$ fluctuations, including drops back to 0‰, e.g. at ~400 Ma,

the long-term mean $\delta^{13}C$ remains ~2‰ throughout the rest of the Paleozoic, the Mesozoic, and the early Cenozoic (17), indicating a sustained increase in global organic carbon burial. Such a permanent shift requires a unidirectional driver that kicked-in during the mid-Paleozoic. The evolution of land plants is the obvious candidate, with the first non-vascular plants (ancestors of extant mosses, liverworts and hornworts) colonizing the land in the Mid-Late Ordovician (~470-445 Ma), followed by the first vascular plants in the Silurian (~445-420 Ma) and early Devonian (~420-390 Ma) (figure 1) (18, 19).

Here we hypothesize that the evolution of these earliest land plants permanently increased organic carbon burial causing atmospheric oxygen to approach modern levels by ~400 Ma, and creating a new dynamically stable steady state for the oxygen cycle (where the major long-term O_2 sink from oxidative weathering of ancient organic carbon increased to counterbalance the increased O_2 source). In simple terms, on long timescales, the global organic carbon burial flux is determined by the supply flux of the ultimate limiting nutrient phosphorus from weathering and the (molar) ratio of carbon-to-phosphorus in material that is buried:

$$\text{P weathering flux} \times C_{organic}/P_{total} \text{ burial ratio} = C_{organic} \text{ burial flux}$$

Land plants typically have a much higher molar C/P ratio (~1000) than marine organic matter (~100) due to carbon-rich but phosphorus-poor structural compounds such as sporopollenin, lignin and, in their fungal mycorrhizal symbionts, chitin. Therefore they can support an increased organic carbon burial flux for the same P weathering flux. The P weathering flux is partly tied to bulk silicate weathering, e.g. due to the dissolution of apatite inclusions in silicate rocks, and the silicate weathering flux of alkalinity is in turn set by negative feedback in the long-term carbon cycle, so is ultimately controlled by the degassing input of CO_2 on timescales ≥1 Myr (7, 10). However, plants and their associated mycorrhizal fungi can increase phosphorus weathering (20-22), and this could be sustained on longer timescales if they preferentially weather phosphorus relative to alkalinity.

In existing models, the evolution of trees starting ~385 Ma is assumed to have led to the burial of high C/P organic material in coal swamps (7, 8, 10), potentially augmented by increased phosphorus weathering rates (10). The Carboniferous-Permian peak in coal production has often been attributed to the evolution of lignin synthesis and a lag before the evolution of fungal degradation of lignin (23), but recent work has questioned this (24). Earlier plants possessed lignified ‘woody’ tissue (25), with precursor structures existing in

marine algae before the transition to land (26), and lignin-degrading fungi potentially present before the Carboniferous (24). Carboniferous coals are not dominated by lignin, instead their accumulation was controlled by a combination of climate and tectonics supporting the creation and sedimentary preservation of peat bogs (24, 27). Given that earlier plants developed peatlands (28), and had rock weathering capabilities (20, 21), they could also have affected the global carbon cycle (18, 20).

Results and discussion

To test our hypothesis we revised the COPSE biogeochemical model (10) to better capture the early rise of plants and examine under what conditions it could explain the geochemical data (persistent rise to $\delta^{13}C$ ~2‰ and the appearance of charcoal). The original baseline model (10) predicts early Paleozoic O_2 ~0.23 PAL at a reference time of 445 Ma, supported by an organic carbon burial flux of ~$4x10^{12}$ mol yr^{-1} (about half the present day value) with $\delta^{13}C$ = 0.03‰. In this stable state, oxidative weathering of ancient organic carbon is correspondingly reduced and its sensitivity to changes in O_2 provides a key negative feedback stabilizing O_2. Key assumptions going into altering the forcing of the model are the global extent and associated productivity of early plants, the C/P ratio of plant material that was buried, and their effect (if any) on phosphorus weathering. To help parameterize these factors we drew on a mixture of experiments, existing data, and more detailed spatial modelling.

We used a trait-based spatial model of cryptogamic vegetation (i.e. bryophyte and lichen) cover (29, 30) driven by Late Ordovician climate simulations (31) at different atmospheric CO_2 levels to predict the potential global net primary productivity (NPP) of the early plant biosphere (32). At atmospheric CO_2 = 8 PAL, consistent with Late Ordovician glaciations (20), predicted global NPP is ~19 GtC yr^{-1} (figure 2), ~30% of today. Predicted NPP is sensitive to variations in CO_2 and climate (figure S1), ice sheet cover (figure S2), and O_2 (table S2), but is consistently higher than the 4.3 GtC yr^{-1} (7% of today) estimated elsewhere (33). In the original COPSE model (10), predicted NPP only reaches ~5% of today's value in the Late Ordovician and Silurian, but when we assume a stronger late Ordovician phase of land colonization by non-vascular plants (following (20), see SI), then COPSE predicts global NPP 30-40% of today (figure 3a), consistent with the detailed spatial model. In COPSE, this advent of early land plants alone, with no assumed effect on weathering fluxes, and assumed

C/P=1000, increases total organic carbon burial by ~25%, $\delta^{13}C$ by 0.5‰, and atmospheric O_2 by 0.11 PAL (figure 3, blue).

We undertook a literature review of molar C/P ratios in extant bryophytes (table S3) to test whether C/P=1000 is a reasonable assumption for early plants. This gives a range of C/P=800-4300 with a mean of C/P ~1900. Furthermore, early Devonian coaly shales indicate extensive peatlands 410-400 Ma and have C/N of 44-119 (28), comparable to that in modern peatlands where N/P and C/P ratios tend to increase with depth to C/P >3000 (34). Taken together these data suggest that assuming C/P=1000 for early plants is conservative. If instead we assume that buried early plant matter had C/P=2000, then given their productivity, even with no effect on weathering fluxes, this increases global organic carbon burial by ~50%, $\delta^{13}C$ by 1.1‰ and atmospheric O_2 by 0.27 PAL (figure 3, cyan).

Early plants could also have had a significant effect on weathering fluxes (20), as they and their fungal mycorrhizal symbionts evolved means of accessing rock-bound nutrients, notably phosphorus. Experimental work (20) has shown that a modern non-vascular plant, the moss *Physcomitrella patens* amplifies the weathering of Ca ions 1.4-3.6 fold and Mg ions 1.5-5.4 fold from silicate rocks (granite-andesite), and amplifies the weathering of phosphorus from granite ~24(15-43) fold (see Materials and Methods). Subsequent experiments (21) with the modern liverwort *Marchantia paleacea* found a 2.5-7 fold amplification of Ca weathering and a 9-13 fold amplification of P weathering from basalt. Both studies thus indicate preferential weathering of P relative to Ca and Mg (and corresponding alkalinity). The presence of these rock weathering capabilities in two early-diverging lineages (mosses and liverworts) suggests it is an ancestral trait. It has been argued (21, 33) that such large measured local effects would not have scaled up to significant global effects, because of low global NPP (33) and a limited depth of influence in the soil (21). However, we estimate much higher global NPP (figure 2) and weathering potential (32). We also note that extensive shallow water phosphate deposits in the Late Ordovician (35) indicate a marked increase in phosphorus input to the ocean (20).

If we include in COPSE an effect of early plants on silicate weathering following (20), assuming C/P=1000, this increases organic carbon burial by ~35%, $\delta^{13}C$ by 0.7‰, and O_2 by 0.18 PAL (figure 3, magenta). The effect on O_2 is constrained because atmospheric CO_2 and temperature are reduced (20) such that the silicate weathering flux (and associated phosphorus flux) continues to match the degassing flux of CO_2 (figure S3). However,

increases in carbonate weathering (enhanced by plants) and oxidative weathering (due to the rise in O_2) increase the overall phosphorus weathering flux, roughly doubling the O_2 rise due to terrestrial production of high C/P material alone. Assuming that buried early plant matter had a higher C/P=2000 causes larger increases in total organic carbon burial ~60%, $\delta^{13}C$ +1.2‰, and atmospheric O_2 +0.35 PAL (figure 3, green).

However, to reproduce the observed $\delta^{13}C$ +2‰ excursion requires the inclusion of some selective weathering of phosphorus by early plants. Assuming that early plants caused a sustained 50% increase in phosphorus weathering relative to bulk rock dissolution, with C/P=1000, increases total organic carbon burial by ~95%, $\delta^{13}C$ by 2.2‰ and O_2 by 0.74 PAL (to 0.97 PAL at 417 Ma) (figure 3, yellow). Assuming a sustained 25% increase in phosphorus weathering relative to bulk rock and C/P=2000, increases organic carbon burial by ~90%, $\delta^{13}C$ by 2.1‰ and O_2 by 0.67 PAL (figure 3, red). Alternatively, a series of P weathering spikes designed to reproduce the observed sequence of positive $\delta^{13}C$ excursions (figure 1), combined with C/P=2000, produces a series of spikes in organic carbon burial and a peak increase of O_2 of 0.72 PAL at 407 Ma (figure 3, black). We hypothesize that these assumed weathering spikes could reflect phases of plant colonization (20, 36) followed by the establishment of phosphorus recycling ecosystems (20). However, direct evidence linking a phase of land colonization to enhanced weathering and a positive $\delta^{13}C$ excursion has only thus far been established for the Silurian-Devonian boundary excursion (36). Therefore alternative hypotheses for short-lived positive $\delta^{13}C$ excursions should also be considered.

Regarding the simulated long-term ~2‰ rise in $\delta^{13}C$ this is smaller than would be expected from standard application of the simplified formula: $\delta^{13}C(ocean) = \delta^{13}C(river) + f_{org} \cdot \varepsilon$, where f_{org} is the fraction of carbon buried as organic matter, ε is the fractionation between carbonates and organic matter, and both ε and $\delta^{13}C(river)$ are usually assumed to be constant. In our COPSE simulations there is a fully interactive isotope mass balance and these terms are not constant. The approximate doubling of organic carbon burial (with roughly constant carbonate burial) represents an increase from $f_{org} = 0.18$ to $f_{org} = 0.31$. However, the increase in burial of isotopically-light organic carbon is counteracted by an increase in the oxidative weathering of isotopically-light organic carbon, which lowers the $\delta^{13}C$ of riverine input to the ocean from ca. -5‰ to ca. -7.5‰. This in turn is partially counteracted by an increase in fractionation between carbonates and organic matter from $\varepsilon \sim 27‰$ to $\varepsilon \sim 30‰$, due to increasing O_2 (somewhat counteracted by declining CO_2).

Sensitivity analyses (see SI) indicate that our results are robust. Varying the uplift and degassing forcing of the model within plausible bounds only causes ±0.08 PAL variation in O_2 about the initial state (figure S4), although it does cause the effect of the same early plant forcing scenario to range over +0.4-1.0 PAL O_2 (table S4). Including an additional negative feedback on O_2, from increased marine organic C/P burial ratios under anoxic waters (37), increases its initial early Paleozoic level to 0.54 PAL and reduces the effect of the same biological forcing scenarios on O_2 by ~10-30%, giving a maximum increase of +0.63 PAL (table S5). However, because the initial O_2 is now higher, the final O_2 is also higher in all cases, and even scenarios without selective weathering of phosphorus could explain the appearance of charcoal (O_2 >~0.7 PAL).

Our model makes additional predictions that can be tested against geochemical data, notably it predicts a decline in pyrite sulfur burial and associated drop in $\delta^{34}S$ and increase in seawater [SO_4] and C/S burial ratio with the rise of the earliest plants (figure S5). This is broadly consistent with the sulfur isotope ($\delta^{34}S$) record (38-40), which shows a marked decline through the Silurian-early Devonian from ~30‰ to ~18‰, although available data also suggest an earlier late Ordovician-early Silurian rise from ~25‰ to ~30‰, which the present model does not capture. The model is consistent with proxy reconstructions of seawater [SO_4], which suggest an Ordovician-Silurian rise from ~6 mM to ~10 mM (41), and with a Silurian increase in the molar C/S ratio of shales from ~5 to ~16 (15).

Other processes not yet included in the model warrant future consideration, for example the effect of increasing atmospheric mass on climate (42), and the effect of weathering forcing scenarios on $\delta^{7}Li$ and $^{87}Sr/^{86}Sr$, which enable additional tests against data.

Conclusion

Our model can only reproduce Paleozoic geochemical data if the rise of the earliest land plants caused a major oxygenation event of the Earth's atmosphere and oceans by ~400 Ma. We attribute this mid-Paleozoic oxygenation event to a persistent global increase in organic carbon burial supported by the high C/P ratio of early land plant material, augmented by a plant-driven increase in P weathering flux relative to the weathering flux of alkalinity. The $\delta^{13}C$ record suggests this increase in organic carbon burial was essentially permanent, producing a new dynamically stable state for atmospheric O_2. In this new steady state, oxidative weathering was increased (becoming less sensitive to variations in O_2) and new

fire-mediated negative feedbacks on O_2 were instigated that have played a key role in stabilising atmospheric O_2 concentration up to the present day (22, 43). For the earliest land plants to be responsible for such a major mid-Paleozoic oxygenation event requires that they were much more productive and globally extensive than has been previously assumed (7, 10, 33). This hypothesis makes testable predictions with regard to effects on other biogeochemical cycles, notably sulfur. If it stands up to further scrutiny, then we can infer that the earliest land plants created a stable oxygen-rich atmosphere that was necessary for the subsequent evolution of large, mobile, intelligent animals with a high respiratory oxygen demand – including ourselves.

Materials and Methods:

Data compilation: The early charcoal record (table S1) was compiled from the literature (11, 12, 28, 44-72), utilizing existing compilations (12, 44-47) and checking them where possible against the original sources. This involved some reconciling of disparate results between existing compilations and revision of some erroneous quoted values. Where recalculations were warranted, inertinite percentages were calculated on a mineral-matter-free (mmf) basis, following (45, 47).

The molybdenum isotope record from marine shales was updated from (9) with data from (73, 74). Uncertainties shown in figure 1 represent 2 standard deviation of the mean (analytical precision) plus the propagated uncertainty from matching in-house reference materials to the universal standard NIST SRM 3136 where seawater display $\delta^{98/95}Mo = 2.3‰$ (see (75, 76)). The redox state of the host shales was determined using either Fe-speciation or Mo-enrichment proxies. Euxinic shales are defined (77) by the Fe-speciation proxy when $FeHR/FeT > 0.38$ and $FeP/FeHR > 0.7$ (black circles in figure 1). Euxinic shales are defined (78, 79) by the Mo enrichment proxy when $Mo > 25$ ppm (white circles in figure 1). Ferruginous shales (77) are defined by the Fe speciation proxy when $FeHR/FeT > 0.38$ and $FeP/FeHR < 0.7$.

The carbon isotope record (17) was fitted with a smoothed spline function in Matlab; spline = csaps(age, $\delta^{13}C$, rho), where $\rho = 0.99$ (close to data, but the curve in figure 1 does not go through each data point).

The C/P ratio of extant bryophytes (table S3) was compiled from data in the literature (34, 80-88). Where only values of mg P/g biomass were available, a value of mg C/g biomass =

430 was assumed based on the mean value across 6 bryophyte species from (89). Results for molar C/P ratios are given to 2 significant figures, given the uncertainty in the input data, except where authors themselves provide more precise values.

Ecophysiological model of cryptogamic vegetation: We used a trait-based spatial model of cryptogamic vegetation (i.e. bryophyte and lichen) cover to estimate the potential global net primary productivity (NPP) of the early non-vascular plant biosphere (29, 30). The Late Ordovician (445 Ma, Hirnantian Stage) setup of the model is fully described elsewhere (32). The model is driven by existing Late Ordovician climate simulations (31), conducted at a range of different atmospheric CO_2 and O_2 concentrations. Initially, we assume atmospheric O_2 = 0.6 PAL (~14 vol.%) at 445 Ma, which is consistent with those COPSE model simulations (figure 3d) that go on to produce O_2 levels consistent with the fossil charcoal record. We also initially assume atmospheric CO_2 = 8 PAL, which is a widely quoted value consistent with the occurrence of Hirnantian glaciations at 445 Ma (20), and is consistent with those COPSE model simulations that assume an effect of early plants on silicate weathering following (20). We explored the sensitivity of predicted global NPP to variations in atmospheric CO_2 and corresponding climate state (figure S1), to constraining vegetation cover with extensive Late Ordovician ice sheet cover (figure S2), and to varying O_2 in combination with CO_2 (table S2). The relatively high global NPP results obtained are consistent with present day cryptogamic covers providing ~7% of global NPP, despite making up only 1% of terrestrial vegetation by mass (90), and being restricted to relatively resource-poor habitats, whilst also operating in an atmosphere with a low CO_2/O_2 ratio.

Experimental P weathering calculation: In our previously reported (20) weathering experiments with granite, the mean amounts of phosphate weathered into aqueous solution were: control microcosms = 0.0137 μmol P, biotic microcosms = 0.0726 μmol P. The mean moss biomass in the biotic microcosms was 14.390 mg, which assuming 0.43 gC/g biomass and C/P = 2000 (table S3) suggests 0.26 μmol P in biomass, or for C/P = 1000-4000, 0.13-0.52 μmol P in biomass. This gives a biotic P weathering amplification factor ~24 (range 15-43), whereas previously we suggested up to 60 (20). Clearly these estimates are dominated by the unmeasured P content of biomass. However, the P weathering amplification factor has to be >5.3 (the ratio of dissolved phosphate entering solution in microcosms with moss to those without), which is already considerably greater than the amplification factors for Ca = 1.4 and Mg = 1.5 from granite, indicating selective weathering of P.

COPSE model: We used the COPSE model (10, 20) to study the effects of the early rise of land plants on the coupled biogeochemical cycles of C, O, N, P and S, including the $\delta^{13}C$ record. The model is described in full in (10) and the version used here incorporates the changes in model structure described in (20). The model has several forcing parameters, including solar luminosity, the geological factors degassing (*D*), and uplift (*U*), and the biological forcing factors evolution/colonization (*E*), enhancement of weathering (*W*), selective phosphorus weathering (*F*), and changes to the C/P burial ratio of terrestrially-derived material (*CP*). The geologic and biologic forcing factors are all normalized to 1 at the present day, except C/P = 1000 at present day. Our overall modelling strategy was to try and reproduce key changes in the $\delta^{13}C$ record with plausible biological and geological forcing scenarios, constrained where possible by available data. We focused initially on altering the biological forcing scenario whilst using the original geological forcing scenario. Then in a sensitivity analysis we considered uncertainty in geologic forcing (91), and alternative initial conditions (altering the feedback structure of the model). The forcing scenarios and sensitivity analyses are detailed in the SI Materials and Methods.

Acknowledgements:

We thank two anonymous referees for their insightful comments that improved the manuscript. T.M.L., S.J.D. and B.M. were supported by the Leverhulme Trust (RPG-2013-106). T.M.L. was also supported by NERC (NE/I005978/2) and by a Royal Society Wolfson Research Merit Award. T.W.D. was supported by the VILLUM Foundation (VKR023127).

Author contributions:

T.M.L. designed research. T.M.L. and P.P. performed modelling. S.J.D., B.M. and K.O. helped develop the COPSE model and scenarios. T.W.D., M.R.S., K.O. and P.P. provided data and helped analyze it. T.M.L. wrote the paper with input from all co-authors.

References:

1. Canfield DE (2014) Proterozoic Atmospheric Oxygen. *Treatise on Geochemistry. 2nd Edition*, eds Holland HD & Turekian KK (Elsevier Science, Oxford), Vol 6, pp 197-216.

2. Lyons TW, Reinhard CT, & Planavsky NJ (2014) The rise of oxygen in Earth's early ocean and atmosphere. *Nature* 506(7488):307-315.
3. Lenton TM, Boyle RA, Poulton SW, Shields GA, & Butterfield NJ (2014) Co-evolution of eukaryotes and ocean oxygenation in the Neoproterozoic era. *Nature Geoscience* 7(4):257-265.
4. Shields-Zhou GA & Och LM (2011) The case for a Neoproterozoic Oxygenation Event: Geochemical evidence and biological consequences. *GSA Today* 21(3):4-11.
5. Och LM & Shields-Zhou GA (2012) The Neoproterozoic oxygenation event: Environmental perturbations and biogeochemical cycling. *Earth-Science Reviews* 110(1-4):26-57.
6. Sperling EA*, et al.* (2015) Statistical analysis of iron geochemical data suggests limited late Proterozoic oxygenation. *Nature* 523(7561):451-454.
7. Berner RA (2006) GEOCARBSULF: A combined model for Phanerozoic atmospheric O2 and CO2. *Geochimica et Cosmochimica Acta* 70(23):5653-5664.
8. Berner RA & Canfield DE (1989) A new model for atmospheric oxygen over Phanerozoic time. *American Journal of Science* 289:333-361.
9. Dahl TW*, et al.* (2010) Devonian rise in atmospheric oxygen correlated to the radiations of terrestrial plants and large predatory fish. *PNAS* 107:17911-17915.
10. Bergman NM, Lenton TM, & Watson AJ (2004) COPSE: a new model of biogeochemical cycling over Phanerozoic time. *Am. J. Sci.* 304:397-437.
11. Glasspool IJ, Edwards D, & Axe L (2004) Charcoal in the Silurian as evidence for the earliest wildfire. *Geology* 32(5):381-383.
12. Scott AC & Glaspool IJ (2006) The diversification of Paleozoic fire systems and fluctuations in atmospheric oxygen concentration. *Proceedings of the National Academy of Sciences of the United States of America* 103(29):10861-10865.
13. Belcher CM & McElwain JC (2008) Limits for Combustion in Low O2 Redefine Paleoatmospheric Predictions for the Mesozoic. *Science* 321(5893):1197-1200.
14. Hadden RM, Rein G, & Belcher CM (2013) Study of the competing chemical reactions in the initiation and spread of smouldering combustion in peat. *Proceedings of the Combustion Institute* 34(2):2547-2553.
15. Berner RA & Raiswell R (1983) Burial of organic carbon and pyrite sulfur in sediments over phanerozoic time: a new theory. *Geochimica et Cosmochimica Acta* 47(5):855-862.

16. Kump LR (2014) Hypothesized link between Neoproterozoic greening of the land surface and the establishment of an oxygen-rich atmosphere. *Proceedings of the National Academy of Sciences* 111(39):14062-14065.
17. Saltzman MR & Thomas E (2012) Chapter 11 - Carbon Isotope Stratigraphy. *The Geologic Time Scale*, eds Gradstein FM, Schmitz JGOD, & Ogg GM (Elsevier, Boston), pp 207-232.
18. Kenrick P, Wellman CH, Schneider H, & Edgecombe GD (2012) A timeline for terrestrialization: consequences for the carbon cycle in the Palaeozoic. *Phil. Trans. B* 367(1588):519-536.
19. Edwards D, Morris JL, Richardson JB, & Kenrick P (2014) Cryptospores and cryptophytes reveal hidden diversity in early land floras. *New Phytologist* 202(1):50-78.
20. Lenton TM, Crouch M, Johnson M, Pires N, & Dolan L (2012) First plants cooled the Ordovician. *Nature Geoscience* 5(2):86-89.
21. Quirk J*, et al.* (2015) Constraining the role of early land plants in Palaeozoic weathering and global cooling. *Proceedings of the Royal Society of London B: Biological Sciences* 282(1813).
22. Lenton TM & Watson AJ (2000b) Redfield revisited: 2. What regulates the oxygen content of the atmosphere? *Global Biogeochemical Cycles* 14(1):249-268.
23. Robinson JM (1990) Lignin, land plants, and fungi: Biological evolution affecting Phanerozoic oxygen balance. *Geology* 15:607-610.
24. Nelsen MP, DiMichele WA, Peters SE, & Boyce CK (2016) Delayed fungal evolution did not cause the Paleozoic peak in coal production. *Proceedings of the National Academy of Sciences* 113(9):2442-2447.
25. Gerrienne P*, et al.* (2011) A Simple Type of Wood in Two Early Devonian Plants. *Science* 333(6044):837.
26. Labeeuw L, Martone P, Boucher Y, & Case R (2015) Ancient origin of the biosynthesis of lignin precursors. *Biol Direct* 10(1):1-21.
27. Montañez IP (2016) A Late Paleozoic climate window of opportunity. *Proceedings of the National Academy of Sciences* 113(9):2334-2336.
28. Kennedy KL*, et al.* (2013) Lower Devonian coaly shales of northern New Brunswick, Canada: plant accumulations in the early stages of Terrestrial colonization. *Journal of Sedimentary Research* 83(12):1202-1215.

29. Porada P, Weber B, Elbert W, Poschl U, & Kleidon A (2013) Estimating global carbon uptake by lichens and bryophytes with a process-based model. *Biogeosciences* 10(11):6989-7033.
30. Porada P, Weber B, Elbert W, Pöschl U, & Kleidon A (2014) Estimating impacts of lichens and bryophytes on global biogeochemical cycles. *Global Biogeochemical Cycles*:DOI: 10.1002/2013GB004705.
31. Pohl A, Donnadieu Y, Le Hir G, Buoncristiani JF, & Vennin E (2014) Effect of the Ordovician paleogeography on the (in)stability of the climate. *Clim. Past* 10(6):2053-2066.
32. Porada P, *et al.* (2016) High potential for weathering and climate effects of non-vascular vegetation in the Late Ordovician. *Nature Communications* 7:10.1038/ncomms12113.
33. Edwards D, Cherns L, & Raven JA (2015) Could land-based early photosynthesizing ecosystems have bioengineered the planet in mid-Palaeozoic times? *Palaeontology* 58(5):803-837.
34. Wang M, Moore TR, Talbot J, & Richard PJH (2014) The cascade of C:N:P stoichiometry in an ombrotrophic peatland: from plants to peat. *Environmental Research Letters* 9(2):024003.
35. Pope MC & Steffen JB (2003) Widespread, prolonged late Middle to Late Ordovician upwelling in North America: A proxy record of glaciation? *Geology* 31(1):63-66.
36. Małkowski K & Racki G (2009) A global biogeochemical perturbation across the Silurian–Devonian boundary: Ocean–continent–biosphere feedbacks. *Palaeogeography, Palaeoclimatology, Palaeoecology* 276(1–4):244-254.
37. Van Cappellen P & Ingall ED (1996) Redox stabilisation of the Atmosphere and Oceans by Phosphorus-Limited Marine Productivity. *Science* 271:493-496.
38. Prokoph A, Shields GA, & Veizer J (2008) Compilation and time-series analysis of a marine carbonate δ18O, δ13C, 87Sr/86Sr and δ34S database through Earth history. *Earth-Science Reviews* 87(3–4):113-133.
39. Gill BC, Lyons TW, & Saltzman MR (2007) Parallel, high-resolution carbon and sulfur isotope records of the evolving Paleozoic marine sulfur reservoir. *Palaeogeography, Palaeoclimatology, Palaeoecology* 256(3–4):156-173.
40. Jones DS & Fike DA (2013) Dynamic sulfur and carbon cycling through the end-Ordovician extinction revealed by paired sulfate–pyrite δ34S. *Earth and Planetary Science Letters* 363:144-155.

41. Algeo TJ, Luo GM, Song HY, Lyons TW, & Canfield DE (2015) Reconstruction of secular variation in seawater sulfate concentrations. *Biogeosciences* 12(7):2131-2151.
42. Poulsen CJ, Tabor C, & White JD (2015) Long-term climate forcing by atmospheric oxygen concentrations. *Science* 348(6240):1238-1241.
43. Kump LR (1988) Terrestrial feedback in atmospheric oxygen regulation by fire and phosphorus. *Nature* 335:152-154.
44. Rimmer SM, Hawkins SJ, Scott AC, & Cressler WL (2015) The rise of fire: Fossil charcoal in late Devonian marine shales as an indicator of expanding terrestrial ecosystems, fire, and atmospheric change. *American Journal of Science* 315(8):713-733.
45. Glasspool IJ & Scott AC (2010) Phanerozoic concentrations of atmospheric oxygen reconstructed from sedimentary charcoal. *Nature Geosci* 3(9):627-630.
46. Diessel CFK (2010) The stratigraphic distribution of inertinite. *International Journal of Coal Geology* 81(4):251-268.
47. Glasspool IJ, Scott AC, Waltham D, Pronina NV, & Shao L (2015) The impact of fire on the Late Paleozoic Earth System. *Frontiers in Plant Science* 6.
48. Edwards D & Axe L (2004) Anatomical Evidence in the Detection of the Earliest Wildfires. *Palaios* 19(2):113-128.
49. Glasspool IJ, Edwards D, & Axe L (2006) Charcoal in the Early Devonian: A wildfire-derived Konservat–Lagerstätte. *Review of Palaeobotany and Palynology* 142(3–4):131-136.
50. Pflug HD & Prossl KF (1989) Palynology in Gneiss - Results from the Continental Deep Drilling Program. *Naturwissenschaften* 76:565-567.
51. Pflug HD & Prössl KF (1991) Palynostratigraphical and paleobotanical studies in the pilot hole of the German continental deep drilling programme results and implications. *Scientific Drilling* 2:13-33.
52. Wollenweber J*, et al.* (2006) Characterisation of non-extractable macromolecular organic matter in Palaeozoic coals. *Palaeogeography, Palaeoclimatology, Palaeoecology* 240(1–2):275-304.
53. Peppers RA & Damberger HH (1969) Palynology and Petrography of a Middle Devonian Coal in Illinois. (Illinois State Geological Survey, Urbana, Illinois 61801).
54. Ammosov IL (1964) Composition pétrographique des charbons humiques de U.R.S.S. *CR 5eme Congr. Internat. Stratig. Géol. Carbonif. Paris 9-12 Sept. 1963*), Vol 4, pp 1-151.

55. Volkova IB (1994) Nature and composition of the Devonian coals of Russia. *Energy Fuels* 8:1489-1493.
56. Patrakov YF, Kamyanov VF, & Fedyaeva ON (2005) A structural model of the organic matter of Barzas liptobiolith coal. *Fuel* 84(2–3):189-199.
57. Sharypov VI, Kuznetsov BN, Beregovtsova NG, Startsev AN, & Parmon VN (2006) Catalytic hydroliquefaction of Barzass liptobiolitic coal in a petroleum residue as a solvent. *Fuel* 85(7–8):918-922.
58. Ghori KAR (1999) Silurian-Devonian petroleum source-rock potential and thermal history, Carnarvon Basin, Western Australia. (Geological Survey of Western Australia, Perth), p 87.
59. Xu H-H*, et al.* (2012) Mid Devonian megaspores from Yunnan and North Xinjiang, China: Their palaeogeographical and palaeoenvironmental significances. *Palaeoworld* 21(1):11-19.
60. Yang Y, Zou R, Shi Z, & Jiang R (1996) *Atlas for Coal Petrography of China* (China University of Mining and Technology Press, Beijing).
61. Dai S, Han D, & Chou C-L (2006) Petrography and geochemistry of the Middle Devonian coal from Luquan, Yunnan Province, China. *Fuel* 85(4):456-464.
62. Goodarzi F, Gentzis T, & Embry AF (1989) Organic petrology of two coal-bearing sequences from the Middle to Upper Devonian of Melville Island, Arctic Canada. *Geological Survey of Canada Paper* 89-8:120-130.
63. Goodarzi F & Goodbody Q (1990) Nature and depositional environment of Devonian coals from western Melville island, Arctic Canada. *International Journal of Coal Geology* 14(3):175-196.
64. Gentzis T & Goodarzi F (1991) Petrology, depositional environment and utilization potential of Devonian channel coals from Melville Island, Canadian Arctic Islands. *Bulletin de la Societe Geologique de France* 162(2):239-253.
65. Fowler MG, Goodarzi F, Gentzis T, & Brooks PW (1991) Hydrocarbon potential of Middle and Upper Devonian coals from Melville Island, Arctic Canada. *Organic Geochemistry* 17(6):681-694.
66. Michelsen JK & Khorasani GK (1991) A regional study on coals from Svalbard; organic facies, maturity and thermal history. *Bulletin de la Societe Geologique de France* 162(2):385-397.
67. Rimmer SM, Thompson JA, Goodnight SA, & Robl TL (2004) Multiple controls on the preservation of organic matter in Devonian–Mississippian marine black shales:

geochemical and petrographic evidence. *Palaeogeography, Palaeoclimatology, Palaeoecology* 215(1–2):125-154.

68. Marynowski L & Filipiak P (2007) Water column euxinia and wildfire evidence during deposition of the Upper Famennian Hangenberg event horizon from the Holy Cross Mountains (central Poland). *Geological Magazine* 144(03):569-595.
69. Cressler WL (2001) Evidence of earliest known wildfires. *Palaios* 16(2):171-174.
70. Rowe NP & Jones TP (2000) Devonian charcoal. *Palaeogeography Palaeoclimatology Palaeoecology* 164(1-4):331-338.
71. Fairon-Demaret M & Hartkopf-Fröder C (2004) Late Famennian plant mesofossils from the Refrath 1 Borehole (Bergisch Gladbach-Paffrath Syncline; Ardennes-Rhenish Massif, Germany). *CFS Courier Forschungsinstitut Senckenberg* 251:89-121.
72. Prestianni C, Decombeix A-L, Thorez J, Fokan D, & Gerrienne P (2010) Famennian charcoal of Belgium. *Palaeogeography, Palaeoclimatology, Palaeoecology* 291(1–2):60-71.
73. Zhou L, *et al.* (2011) A new paleoenvironmental index for anoxic events—Mo isotopes in black shales from Upper Yangtze marine sediments. *Sci. China Earth Sci.* 54(7):1024-1033.
74. Herrmann AD, *et al.* (2012) Anomalous molybdenum isotope trends in Upper Pennsylvanian euxinic facies: Significance for use of δ98Mo as a global marine redox proxy. *Chemical Geology* 324–325:87-98.
75. Goldberg T, *et al.* (2013) Resolution of inter-laboratory discrepancies in Mo isotope data: an intercalibration. *Journal of Analytical Atomic Spectrometry* 28(5):724-735.
76. Nägler TF, *et al.* (2014) Proposal for an International Molybdenum Isotope Measurement Standard and Data Representation. *Geostandards and Geoanalytical Research* 38(2):149-151.
77. Canfield DE, Poulton SW, & Narbonne GM (2007) Late-Neoproterozoic Deep-Ocean Oxygenation and the Rise of Animal Life. *Science* 315:92-95.
78. Scott C & Lyons TW (2012) Contrasting molybdenum cycling and isotopic properties in euxinic versus non-euxinic sediments and sedimentary rocks: Refining the paleoproxies. *Chemical Geology* 324–325:19-27.
79. Dahl TW, *et al.* (2013) Tracing euxinia by molybdenum concentrations in sediments using handheld X-ray fluorescence spectroscopy (HHXRF). *Chemical Geology* 360–361:241-251.

80. Chapin FS, Johnson DA, & McKendrick JD (1980) Seasonal Movement of Nutrients in Plants of Differing Growth Form in an Alaskan Tundra Ecosystem: Implications for Herbivory. *Journal of Ecology* 68(1):189-209.
81. Chapin FS (1989) The Cost of Tundra Plant Structures: Evaluation of Concepts and Currencies. *The American Naturalist* 133(1):1-19.
82. Chapin FS & Shaver GR (1989) Differences in Growth and Nutrient use Among Arctic Plant Growth Forms. *Functional Ecology* 3(1):73-80.
83. Shaver GR & Chapin FS (1991) Production: Biomass Relationships and Element Cycling in Contrasting Arctic Vegetation Types. *Ecological Monographs* 61(1):1-31.
84. Aerts R, Verhoeven JTA, & Whigham DF (1999) Plant-Mediated Controls on Nutrient Cycling in Temperate Fens and Bogs. *Ecology* 80(7):2170-2181.
85. Riis T, Olesen B, Katborg CK, & Christoffersen KS (2010) Growth Rate of an Aquatic Bryophyte (Warnstorfia fluitans (Hedw.) Loeske) from a High Arctic Lake: Effect of Nutrient Concentration. *Arctic* 63(1):100-106.
86. Waite M & Sack L (2011) Does global stoichiometric theory apply to bryophytes? Tests across an elevation × soil age ecosystem matrix on Mauna Loa, Hawaii. *Journal of Ecology* 99(1):122-134.
87. Wang M & Moore T (2014) Carbon, Nitrogen, Phosphorus, and Potassium Stoichiometry in an Ombrotrophic Peatland Reflects Plant Functional Type. *Ecosystems* 17(4):673-684.
88. Larmola T*, et al.* (2014) Methanotrophy induces nitrogen fixation during peatland development. *Proceedings of the National Academy of Sciences* 111(2):734-739.
89. Delgado V, Ederra A, & Santamaría JM (2013) Nitrogen and carbon contents and δ15N and δ13C signatures in six bryophyte species: assessment of long-term deposition changes (1980–2010) in Spanish beech forests. *Global Change Biology* 19(7):2221-2228.
90. Elbert W*, et al.* (2012) Contribution of cryptogamic covers to the global cycles of carbon and nitrogen. *Nature Geosci* 5(7):459-462.
91. Royer DL, Donnadieu Y, Park J, Kowalczyk J, & Goddéris Y (2014) Error analysis of CO2 and O2 estimates from the long-term geochemical model GEOCARBSULF. *American Journal of Science* 314(9):1259-1283.

Figure legends

Fig. 1. Global changes during the Ordovician, Silurian, and Devonian Periods. The rise of non-vascular plants (indicated by cryptospore diversity (32)) then vascular plants (indicated by trilete spore diversity (18)) overlaps with the first appearances of fossil charcoal (table S1); F = fossils, black dots = inertinite in coal, nd = none detected. Molybdenum isotope data (9) indicate oxygenation of the deep ocean, following an uncertain trajectory ~440-390 Ma; black circles = euxinic shales as defined by Fe-speciation, white circles = euxinic shales as defined by Mo-enrichment, grey triangles = ferruginous shales as defined by Fe-speciation, blue area = isotope offset from oceanic input that requires a substantial Mn-oxide sink in the deep oceans. The carbonate carbon isotope record (17) (red dots, black line is a smoothed spline fit) indicates elevated organic carbon burial ($\delta^{13}C$ ~2‰) ~445-410 Ma. Cm=Cambrian, Fu=Furongian, Llan=Llandovery, W=Wenlock, L=Ludlow, P=Pridoli.

Fig. 2. Predicted Late Ordovician (445 Ma) net primary production (NPP). Result from ecophysiological model of cryptogamic vegetation cover driven by simulated Late Ordovician (445 Ma) climate, atmospheric CO_2 = 8 PAL, and atmospheric O_2 = 0.6 PAL (14 vol.%), with no ice sheet mask. Simulated global NPP = 18.7 GtC yr^{-1}.

Fig. 3. Predictions of mid-Paleozoic global carbon cycle change due to early plants from the updated COPSE model: **a.** Net primary production (NPP); **b.** Organic carbon burial (both terrestrial and marine derived material); **c.** Carbonate carbon isotope record ($\delta^{13}C$); **d.** Atmospheric O_2. Note that fossil charcoal 420-400 Ma indicates O_2 > 0.66-0.77 PAL. (Further results of the same model runs are in figures S3 and S5.) Black dashed = original baseline model run. Blue = early plant colonization (C/P=1000). Cyan = early plant colonization + C/P=2000. Magenta = early plant colonization + biotic effects on silicate weathering (C/P=1000). Green = early plant colonization + C/P=2000 + biotic effects on silicate weathering. Yellow = early plant colonization + biotic effects on silicate weathering + 50% increase in P weathering. Red = early plant colonization + C/P=2000 + biotic effects on silicate weathering + 25% increase in P weathering. Black = early plant colonization + C/P=2000 + biotic effects on silicate weathering + spikes of P weathering.

Fig. 1.

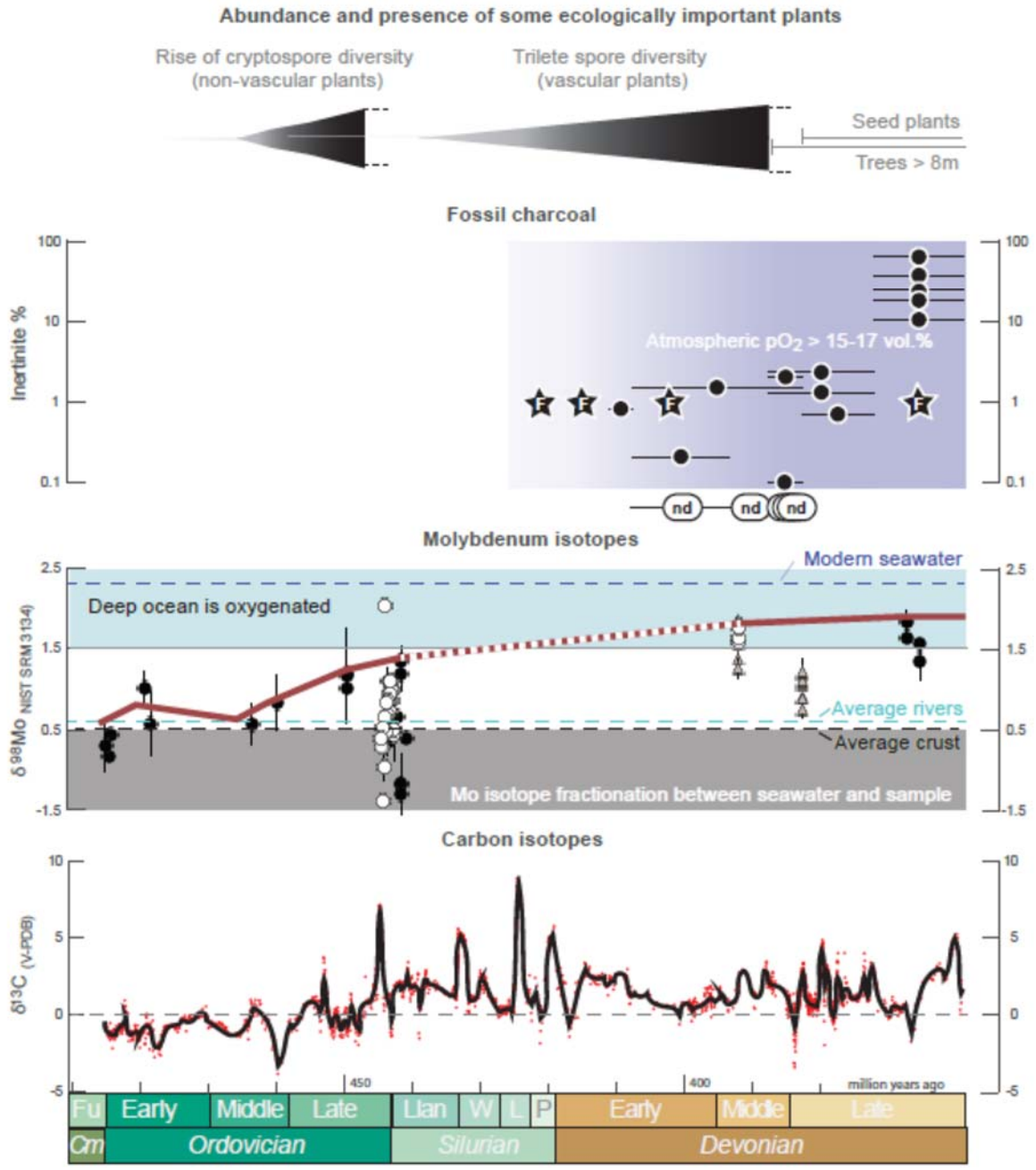
Abundance and presence of some ecologically important plants
Rise of cryptospore diversity
(non-vascular plants)
Trilete spore diversity
(vascular plants)
Seed plants
Trees > 8m
Fossil charcoal
Inertinite %
100
10
1
0.1
Atmospheric pO2 > 15-17 vol.%
nd
nd
nd
Molybdenum isotopes
Modern seawater
Deep ocean is oxygenated
Average rivers
Average crust
Mo isotope fractionation between seawater and sample
δ98MO NIST SRM 3134)
2.5
1.5
0.5
-1.5
Carbon isotopes
δ13C (V-PDB)
10
5
0
-5
450
400
million years ago
Fu
Early
Middle
Late
Llan
W
L
P
Early
Middle
Late
Cm
Ordovician
Silurian
Devonian

Fig. 2.

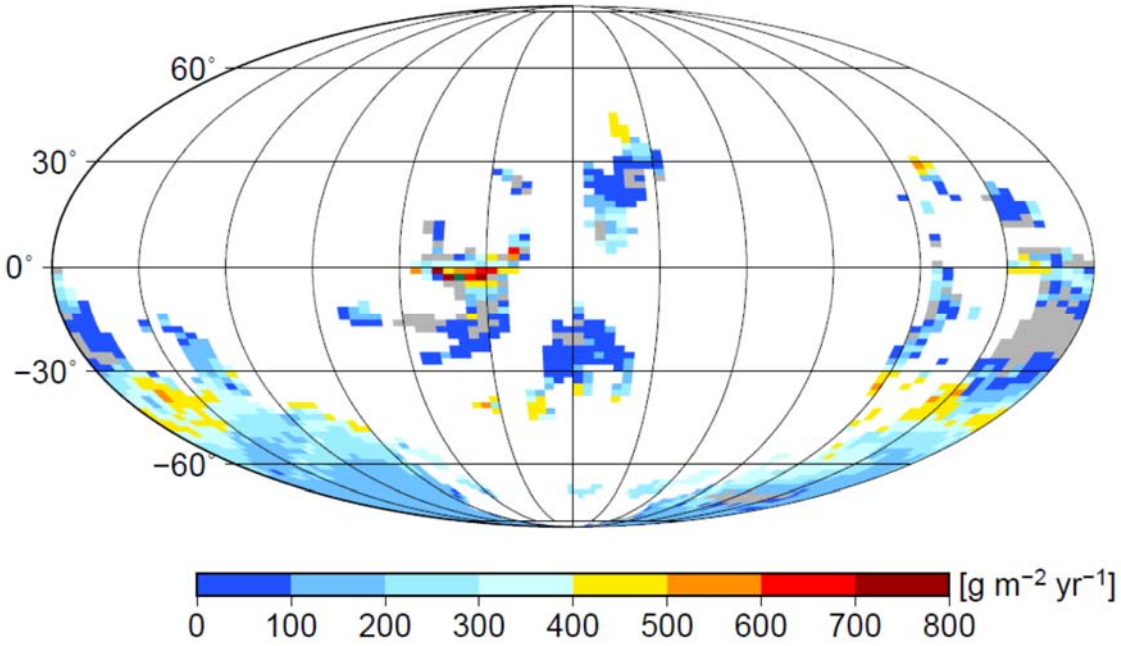

Fig. 3.

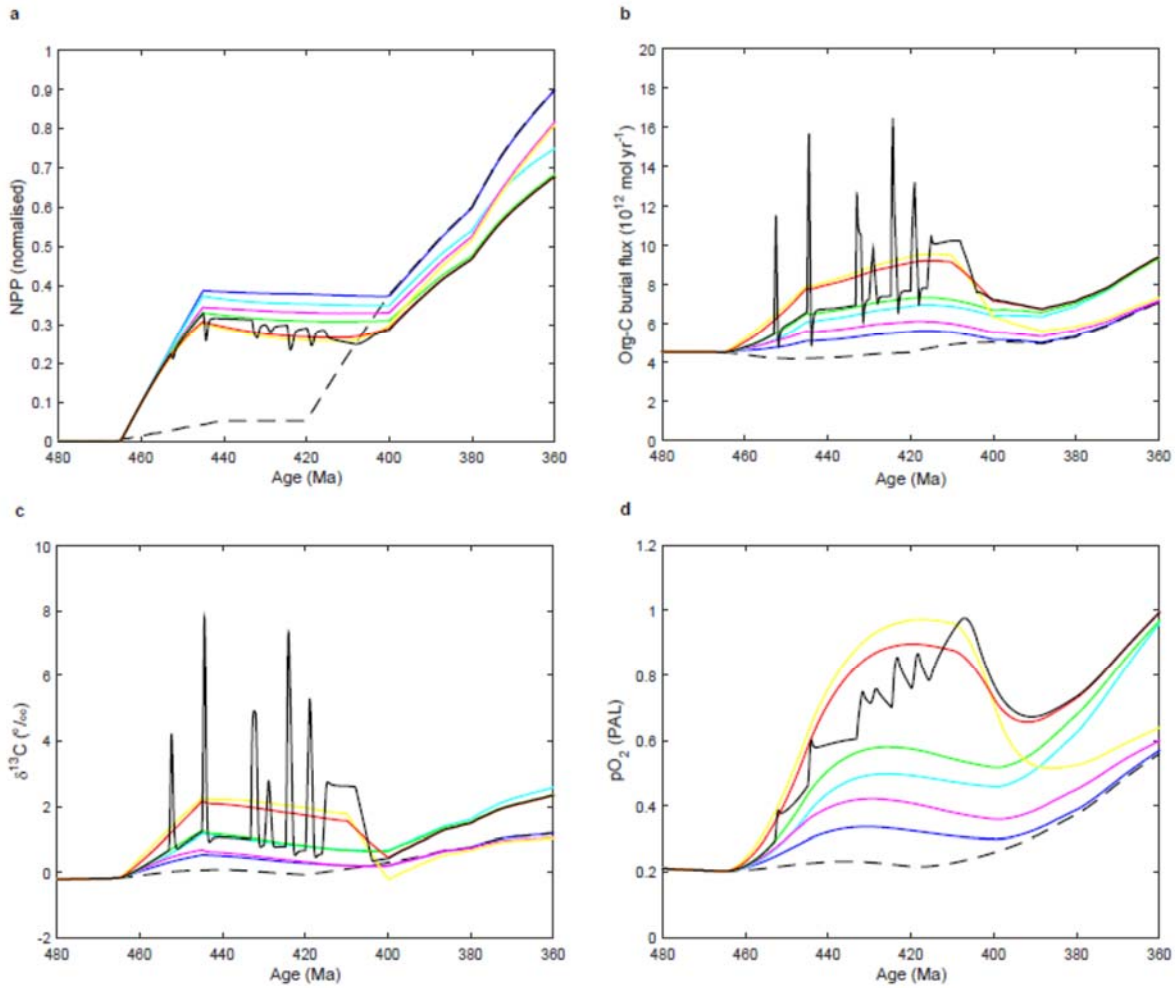
a
NPP (nomalised)
Age (Ma)
b
Org-C burial flux (10^{12} mol yr^{-1})
Age (Ma)
c
$\delta^{13}C$ (‰)
Age (Ma)
d
pO_2 (PAL)
Age (Ma)

SI Materials and Methods

Biological forcing scenarios. We use several different runs of the COPSE model, in which we alter individually and in combination the different biological forcing factors, to explore the potential effects of early plants. The scenarios are based on previous work (20) but updated and extended to span the interval of the Late Ordovician-Silurian-Early Devonian. Our reference scenario is:

(**B**) Baseline run: This is the original model (10) prescription of changing solar, geological and biological forcing over the focal interval. This includes very subtle early plant colonization $E = 0 \rightarrow 0.02$ over 465-440 Ma, constant until 420 Ma, then $E = 0.02 \rightarrow 0.15$ over 420-400 Ma, which is combined with $W = 0 \rightarrow 0.02$ over 465-440 Ma, constant until 420 Ma, then $W = 0.02 \rightarrow 0.1$ over 420-400 Ma. As E and W are effectively multiplied together in the weathering equations of the model (10), the resulting effects on weathering are tiny. However, the rise of E combined with C/P = 1000 causes a small burial flux of terrestrial organic matter ~0.2×10^{12} mol/yr up to 420 Ma, rising to ~1.2×10^{12} mol/yr at 400 Ma and ~1.5×10^{12} mol/yr at 390 Ma. This has no significant effect on O_2 until after 420 Ma, but it does cause O_2 to rise from 0.22-0.23 PAL at 420-410 Ma to ~0.26 PAL at 400 Ma and ~0.31 PAL at 390 Ma. (For this reason the effect of the following scenarios on O_2 tends to be greatest at 420-410 Ma.)

In adjusting from the reference scenario we first add:

(**E**) Early plant colonization: The forcing parameter E was altered to explore the effects of early plant evolution/colonization. We assume: $E = 0$ up to 465 Ma then linear rise to $E = 0.15$ at 445 Ma, remaining constant until 400 Ma, where it joins with the original scenario. This is the same magnitude of change in E as in (20) but is slightly later in timing (previously the increase in E was imposed over 475-460 Ma), partly reflecting updates to the geologic timescale for this interval.

We then add different biological effects to scenario (E), either individually or in combination:

(**CP**) Effects on C/P burial ratio: The molar C/P burial ratio of terrestrially-derived organic matter was altered to explore the effects of the high C/P ratio observed in extant bryophytes and the peats that they produce (table S3). We assume an increase from C/P = 1000 to C/P = 2000 over 465-445 Ma, constant thereafter, which re-joins the original scenario at 345 Ma. (Later on C/P declines to 1000 which is assumed to be due to the evolution of lignin degrading fungi and a decline in coal-producing peatlands.)

(**W**) Effects on silicate (and carbonate) weathering: The forcing parameter *W* was altered to explore the effects of early plant enhancement of silicate (and carbonate) weathering. We assume: $W = 0$ up to 465 Ma then linear rise to $W = 0.75$ at 445 Ma, then constant, re-joining the original scenario at ~300 Ma. This is the same increase in *W* as in (20) just somewhat later in timing.

(**F**) Effects on phosphorus weathering: The forcing parameter *F* was increased to explore the effects of selective weathering of phosphorus by early plants in an attempt to try and reproduce the timing of key changes in the $\delta^{13}C$ record. We explore several variants:

(**i**) In an attempt to capture the +2‰ plateau in $\delta^{13}C$ we assume: $F = 1$ up to 465 Ma then linear rise to $F = 1.5$ at 445 Ma, held constant over 445-410 Ma, then a linear reduction back to $F = 1$ at 400 Ma.

(**ii**) As (i) but increasing to $F = 1.25$ (for use with C/P = 2000).

(**iii**) Spikes of phosphorus weathering: Sharp increases then decreases of phosphorus weathering were introduced to reproduce the positive excursions in the $\delta^{13}C$ record known as the 'GICE', 'HICE', 'Ireviken', 'Mulde', 'Lau', and 'Klonk' events, and a pronounced early Devonian positive excursion. These short duration perturbations are conceived here as possible phases of land colonization involving weathering of relatively bare rock terrains, followed by the establishment of phosphorus recycling soil systems with an attendant drop in the flux of phosphorus weathering. Their timing and duration was based on the latest carbon isotope stratigraphy(17). The spikes we impose are: (GICE) $F = 1 \rightarrow 2.5 \rightarrow 1$ over $453 \rightarrow 452.5 \rightarrow 452$ Ma, (HICE) $F = 1 \rightarrow 3.5 \rightarrow 1$ over $445 \rightarrow 444.5 \rightarrow 444$ Ma, (Ireviken) $F = 1 \rightarrow 2 \rightarrow 2 \rightarrow 1$ over $433.25 \rightarrow 433 \rightarrow 432 \rightarrow 431.5$ Ma, (Mulde) $F = 1 \rightarrow 1.5 \rightarrow 1$ over $430 \rightarrow 429 \rightarrow 428$ Ma, (Lau) $F = 1 \rightarrow 3 \rightarrow 1$ over $424.75 \rightarrow 424.25 \rightarrow 423$ Ma, (Klonk) $F = 1 \rightarrow 2.25 \rightarrow 1$ over $420 \rightarrow 419 \rightarrow 418$ Ma, (early Devonian) $F = 1 \rightarrow 1.5 \rightarrow 1.5 \rightarrow 1$ over $416 \rightarrow 415 \rightarrow 408 \rightarrow 404$ Ma. (The early 'GICE' and 'HICE' spikes contrast in timing and duration somewhat from ref. (20) where $F = 1 \rightarrow 2 \rightarrow 1$ over $460 \rightarrow 458 \rightarrow 456$ Ma, and $F = 1 \rightarrow 3 \rightarrow 1$ over $447 \rightarrow 445 \rightarrow 443$ Ma, due to updates of the geological timescale and carbon isotope stratigraphy in this interval.)

Results for these scenarios are given in figures 3, S3, S5, and some are given in table S5 where changes in total organic carbon burial flux ($F_{Org\text{-}C}$), $\delta^{13}C$ and atmospheric CO_2 are given at 445 Ma, which is typically a minor peak in $F_{Org\text{-}C}$ and the time of maximum change in $\delta^{13}C$ and atmospheric CO_2, whereas quoted peak changes in atmospheric O_2 occur later.

Geological forcing sensitivity analysis. The original geologic forcing scenario over the late Ordovician-Silurian-early Devonian (460-400 Ma) has a generally high level of degassing *D* ~1.5 (with a slight rise and then fall) relative to today, consistent with it being an interval of high levels of volcanic activity and formation of subduction zones. The original uplift forcing *U* is more variable dropping from *U* ~1.08 at 470 Ma, to a minimum *U* =0.84 at 440 Ma, increasing to a maximum *U* =1.04 at 410 Ma, then dropping again to *U* ~0.8 at 390-380 Ma. This two peak structure can be related to the main phases of mountain building of the Taconic orogeny and the Caledonian (Acadian) orogeny, separated by a more quiescent interval in the early Silurian. However, the imposed drop in uplift *U* in the Mid to Late Ordovician, was originally inferred from a significant drop in the $^{87}Sr/^{86}Sr$ composition of seawater, which could also have been due to extensive weathering of volcanic rocks with low $^{87}Sr/^{86}Sr$ composition, at a time of significant ongoing uplift associated with the Taconic orogeny.

To explore the consequences of uncertainty in the geologic (degassing and uplift) forcing of the model, we undertake a sensitivity analysis based on that conducted by Royer et al. (91) using the GEOCARBSULF model, but with an expanded uncertainty range. Their uncertainty range on spreading rate over time, which is equivalent to degassing, is +/-17.5%, whereas for dependence of weathering on relief, which is equivalent to uplift, it is only +/-8% (because the GEOCARBSULF model tends to crash under wider ranges in input parameters). We opt for a consistent +/-20% uncertainty range on both parameters, *D* and *U*, either side of the best guess trajectories for them from (91). The default degassing trajectory is similar to the original COPSE degassing forcing, whereas the default uplift trajectory is much smoother and only captures very long timescale variation with the supercontinent cycle. Nevertheless, a +/-20% uncertainty range produces an envelope which encompasses the more temporally variable original COPSE uplift forcing (figure S4a,b).

With the central estimates for degassing and uplift forcing from Royer et al. (91), the baseline run of the model is subtly altered during the focal interval 480-380 Ma (figure S4c-f), due to the smoothing out of the uplift forcing, but the effects on organic carbon burial, $\delta^{13}C$ (<0.1‰), and atmospheric O_2 (~0.02 PAL) are small. Results of the sensitivity analysis for varying geological forcing are summarized in table S4, where all results are given relative to the original baseline (including the effects of the new baseline geological forcing relative to the original baseline). Again, changes in total organic carbon burial flux ($F_{Org\text{-}C}$), $\delta^{13}C$ and atmospheric CO_2 are given at 445 Ma, whereas changes in atmospheric O_2 are given at 410 Ma, which is typically close to the time of maximum change in O_2.

Sensitivity to initial O_2 level (and feedback structure). To explore the consequences of uncertainty in the feedback structure of the model, which in turn affects the initial atmospheric O_2 level, we include an anoxia sensitivity of the C/P burial ratio of marine organic matter (37), which acts as a negative feedback on variations in atmospheric O_2. This is equivalent to 'run 2' of the original model (10). Including this feedback increases the baseline Paleozoic atmospheric O_2 level in the model by ~0.3 PAL (e.g. from 0.23 PAL to 0.54 PAL at 420 Ma), by increasing organic carbon burial (and with that $\delta^{13}C$). From this alternative baseline O_2 (and corresponding feedback structure) we explore the same range of biological forcing scenarios detailed above and in the main paper, with the results presented in table S5.

Supplementary Figure Legends

Fig. S1. Dependence of predicted Late Ordovician global net primary productivity (NPP) on atmospheric CO_2 and resultant climate state (assuming atmospheric O_2 = 0.6 PAL or 14 vol.%, and no substantive ice sheet cover).

Fig. S2. Predicted Late Ordovician (445 Ma) net primary production (NPP) constrained by ice sheet cover. Result from ecophysiological model of cryptogamic vegetation cover driven by simulated Late Ordovician (445 Ma) climate, atmospheric CO_2 = 8 PAL, and atmospheric O_2 = 0.6 PAL (14 vol.%), with extensive ice sheet mask (grey-blue). Global NPP = 10.5 GtC yr^{-1}.

Fig. S3. Additional results for the central set of COPSE model runs (as in figure 3): **a.** Atmospheric CO_2; **b.** Global temperature; **c.** Phosphorus weathering flux; **d.** Other weathering fluxes; carbonate (upper), silicate (middle), oxidative (lower). Key as in figure 3.

Fig. S4. Uncertainty ranges on the geologic forcing factors degassing and uplift and their effects on model predictions: **a.** Degassing; **b.** Uplift; **c.** Total organic carbon burial; **d.** Carbonate carbon isotope record ($\delta^{13}C$); **e.** Atmospheric O_2; **f.** Atmospheric CO_2. Original model forcing scenario (black dashed line) compared with Royer central estimates (blue), and extreme combinations of weak degassing and strong uplift (green), and strong degassing and weak uplift (red).

Fig. S5. Sulfur cycle results for the central set of COPSE model runs (as in figure 3): **a.** Pyrite sulfur burial flux; **b.** Marine sulfate sulfur isotope record ($\delta^{34}S$); **c.** Ocean sulfate concentration, [SO_4]; **d.** Ratio of marine organic carbon burial to marine pyrite sulfur burial. Key as in figure 3.

Table S1. Compilation of the Silurian-Devonian charcoal record showing primary sources (Ref.) and existing compilations (2º) used.

Ref.	2º	Type	Stratigraphy	Stage	Age (Ma)	Location	n	Inertinite (% mmf)
(11)	(12, 44)	Fossils	Platyschima Shale Mbr, Downton Fm	Basal Pridoli	423.0-419.2	Ludford Lane, Ludlow, UK		
(48, 49)	(12, 44)	Fossils	Ditton Gp	Early Lochkovian	419.2-410.8	N. Brown Clee Hill, UK		
(50, 51)	(12)	Fossils		Pragian/Emsian	410.8-393.3	KTB core, Bavaria, Germany		
(28)		Coaly shale	Val d'Amour Fm	Pragian	410.8-407.6	New Brunswick, Canada	4	0.8
(28)		Coaly shale	Campbellton Fm	Emsian	407.6-393.3	New Brunswick, Canada	4	0.0
(45)	(45)	Coal	L'Anse-a-Brillant coal	Early Emsian	407.6-393.3	Canada, Gaspe, Tar Point	1	0.2
(52)	(46)	Fossil		Emsian	407.6-393.3	Bad Munstereifel, Germany	1	1.5
(53)	(47)	Coal	Wapsinicon Fm, Davenoport Mbr	Eifelian	393.3-387.7	Illinois, USA	3	0.0
(54-57)	(45, 46)	Coal	Barzas coal	Eifelian-Givetian	393.3-382.7	Barzas, Estonia	4	1.5
(58)	(47)	Coal	Nannyara Sandstone	Givetian	387.7-382.7	Carnarvon Basin, Australia	1	2.0
(58)	(47)	Coal	Nannyara Sandstone	Givetian	387.7-382.7	Carnarvon Basin, Australia	1	0.0
(59)	(47)	Coal	Hujiersite Fm	Givetian	387.7-382.7	North Xinjiang, China	1	0.0
(60)	(45)	Coal		Givetian	387.7-382.7	China		0.0
(61)	(45, 46)	Coal		Givetian	387.7-382.7	Luquan, Yunnan, China	8	0.1
(52)	(45, 46)	Coal		Givetian-Frasnian boundary	382.7	Mimerdalen, Spitsbergen	1	0.0
(62-65)	(12, 44, 45)	Coal	Weatherall Fm	Late Givetian-Mid Frasnian	387.7-372.2	W. Melville Island, Canada	8	1.3
(62-65)	(12, 44, 45)	Coal	Hecla Bay Fm	Late Givetian-Mid Frasnian	387.7-372.2	W. Melville Island, Canada	13	2.3
(62-65)	(12, 44, 45)	Coal	Beverley Inlet Fm	Early-Middle Frasnian	382.7-372.2	W. Melville Island, Canada	6	0.7
(66)	(47)	Coal	Roedvika Fm, Tunheim Mbr, Seam A	Late Famennian	372.2-358.9	Bjornoya, Norway	11	36.7
(66)	(47)	Coal	Roedvika Fm, Tunheim Mbr, Seam B	Late Famennian	372.2-358.9	Bjornoya, Norway	7	61.9
(67)	(12)	Black shale	Huron Shale Mbr, New Albany Shale	Famennian (oldest)	372.2-358.9	D6 core, Kentucky, USA	40	10.3
(67)	(12)	Black shale	Three Lick Bed, New Albany Shale	Famennian (middle)	372.2-358.9	D6 core, Kentucky, USA	3	17.8
(67)	(12)	Black shale	Cleveland Shale Mbr, New Albany S.	Famennian (youngest)	372.2-358.9	D6 core, Kentucky, USA	17	23.7
(44)	(44)	Black shale	New Albany Shale, Ohio Shale	Famennian	372.2-358.9	IRQ, D4, D6, OHLO2 cores		
(68)	(44)	Black shale	Hangenberg Black Shale	Latest Famennian	372.2-358.9	Kowala Quarry, Poland		
(44)	(44)	Fossils	Hampshire Fm	Famennian	372.2-358.9	Elkins, West Virginia, USA		
(69)	(12, 44)	Fossils	Duncannon Mbr, Catskill Fm	Famennian 2c	372.2-358.9	Red Hill, Pennsylvania, USA		
(70)	(12)	Fossils	Hangenberg Sandstein	Late Famennian	372.2-358.9	Oese, Sauerland, Germany		
(71)	(12, 44)	Fossils	Knoppenbissen Fm	Famennian	372.2-358.9	Refrath 1 Borehole, Germany		
(72)	(44)	Fossils	Evieux Fm, Condroz Gp	Late Famennian	372.2-358.9	3 quarries, Belgium		

Table S2. Sensitivity of predicted Late Ordovician global net primary productivity (NPP in GtC yr^{-1}) to atmospheric O_2 and CO_2 combinations (assuming no substantive ice sheet cover).

	O_2 (PAL)		
CO_2 (PAL)	0.2	0.6	1.0
4	8.0	7.8	7.7
8	19.4	18.7	18.3
16	28.1	27.1	26.5

Table S3. Bryophyte C/P ratios from literature review (molar ratios given to 2 s.f. given uncertainty in input data, except where authors provide more precise values).

Species/identifier	n	mg P/g biomass	mg C/g biomass	C/P mass	C/P molar	Ref.
Aulacomnium spp.	6	0.8	430*	540	1400	(80)
Polytrichum spp. + *Pogonatum* spp	6	0.7	430*	610	1600	(80)
Aulacomnium turgidum		1	430*	430	1100	(81)
Hylocomium splendens		0.9	430*	480	1200	(81)
Aulacomnium turgidum	4	1.2	430*	360	920	(82)
Hylocomium splendens	4	1.1	430*	390	1000	(82)
Sphagnum rubrum	4	0.8	430*	540	1400	(82)
bryophyte (tussock site)		1	430*	540	1400	(83)
bryophyte (shrub site)		0.8	430*	330	850	(83)
bryophyte (wet site)		1.3	430*	310	790	(83)
bryophyte (heath site)		1.4	430*	860	2200	(83)
Sphagnum spp.	43	0.56	430*	770	2000	(84)
Warnstorfia fluitans		0.5-2.4	410-470	550-950	1400-2400	(85)
12 species across altitudes & soil ages		0.33-0.63		729-1550	1900-4000	(86)
Sphagnum spp.		0.6-0.8		700-1000	1800-2600	(87)
Sphagnum spp. (foliage)				794	2050	(34)
Sphagnum spp. (litter)				911	2350	(34)
Sphagnum spp. (peat)				1285	3310	(34)
Sphagnum (meadow)		1		515	1330	(88)
Sphagnum (mesotrophic fen flark)		1.6		414	1070	(88)
Sphagnum (mesotrophic fen hummock)		0.8		733	1890	(88)
Sphagnum (oligotrophic fen flark)		0.6		722	1860	(88)
Sphagnum (oligotrophic fen hummock)		0.5		999	2580	(88)
Sphagnum (fen-bog transition flark)		0.4		1376	3550	(88)
Sphagnum (fen-bog transition hummock)		0.3		1655	4270	(88)

*Mean value across 6 bryophyte species from (89)

Table S4. Results of sensitivity analysis varying geologic forcing factors (R = Royer et al. (91), B = Baseline) with or without early plant forcing scenario.

Forcing scenario	Uplift	De-gassing	Biology	$F_{Org\text{-}C}$ (mol/yr)	$\Delta\delta^{13}C$ (‰)	ΔCO_2 (PAL)	ΔO_2 (PAL)
				445 Ma	445 Ma	445 Ma	410 Ma
Original baseline	B	B	B	$4.1x10^{12}$	0	0	0
New baseline	R	R	B	$4.4x10^{12}$	-0.1	-1.3	-0.01
Strong uplift	R+20%	R	B	$4.7x10^{12}$	-0.2	-3.3	-0.04
Weak uplift	R-20%	R	B	$4.1x10^{12}$	0.0	1.4	0.03
Strong degassing	R	R+20%	B	$5.0x10^{12}$	0.0	0.8	0.04
Weak degassing	R	R-20%	B	$3.8x10^{12}$	-0.2	-3.7	-0.05
Strong U, weak D	R+20%	R-20%	B	$4.0x10^{12}$	-0.3	-5.4	-0.08
Weak U, strong D	R-20%	R+20%	B	$4.7x10^{12}$	0.1	3.8	0.08
Original baseline	B	B	E+W+F(i)	$8.0x10^{12}$	2.2	-8.4	0.74*
New baseline	R	R	E+W+F(i)	$8.3x10^{12}$	2.0	-9.6	0.72
Strong uplift	R+20%	R	E+W+F(i)	$8.9x10^{12}$	1.7	-11	0.60
Weak uplift	R-20%	R	E+W+F(i)	$7.6x10^{12}$	2.3	-8.0	0.85
Strong degassing	R	R+20%	E+W+F(i)	$9.5x10^{12}$	2.3	-8.3	0.89
Weak degassing	R	R-20%	E+W+F(i)	$7.1x10^{12}$	1.7	-11	0.51
Strong U, weak D	R+20%	R-20%	E+W+F(i)	$7.5x10^{12}$	1.4	-12	0.40
Weak U, strong D	R-20%	R+20%	E+W+F(i)	$8.7x10^{12}$	2.6	-6.5	1.01

*Note: With the original geologic forcing this peak increase in O_2 occurs earlier at 417 Ma.

Table S5. Results of sensitivity analysis adding a range of biological forcing scenarios to a model with higher baseline O_2 level due to additional negative feedback.

Feedback structure	Biology scenario	F_{Org-C} (mol/yr) 445 Ma	$\Delta\delta^{13}C$ (‰) 445 Ma	ΔCO_2 (PAL) 445 Ma	ΔO_2 (PAL) peak*	O_2 (PAL) peak*
Original baseline	B (baseline)	$4.1x10^{12}$	0 (0.03)	0 (17.2)	0	(0.23)
	E	$5.1x10^{12}$	0.5	-0.6	0.11	0.34
	E+CP	$6.1x10^{12}$	1.1	-1.5	0.27	0.50
	E+W	$5.6x10^{12}$	0.7	-7.5	0.18	0.41
	E+CP+W	$6.5x10^{12}$	1.2	-8.0	0.35	0.58
	E+W+F(i)	$8.0x10^{12}$	2.2	-8.4	0.74	0.97
	E+CP+W+F(ii)	$7.8x10^{12}$	2.1	-8.5	0.67	0.90
	E+CP+W+F(iii)	$6.6x10^{12}$**	1.2**	-7.9**	0.72***	0.97***
$(C/P)_{org} = f(O_2)$	B (baseline)	$6.1x10^{12}$	0.7	0.2	0.31	0.54
	E	$6.6x10^{12}$	1.0	-0.6	0.38	0.61
	E+CP	$7.3x10^{12}$	1.5	-1.2	0.49	0.72
	E+W	$7.1x10^{12}$	1.2	-7.2	0.47	0.70
	E+CP+W	$7.7x10^{12}$	1.6	-7.5	0.57	0.80
	E+W+F(i)	$9.4x10^{12}$	2.9	-7.9	0.96	1.19
	E+CP+W+F(ii)	$9.0x10^{12}$	2.5	-7.9	0.84	1.07
	E+CP+W+F(iii)	$7.7x10^{12}$**	1.5**	-7.4**	0.92***	1.17***

*typically occurs during 430-415 Ma, **this is just before a sharp peak in F_{Org-C} and $\delta^{13}C$ and a sharp minimum in CO_2, ***407 Ma peak when baseline O_2 = 0.25 PAL

Fig. S1.

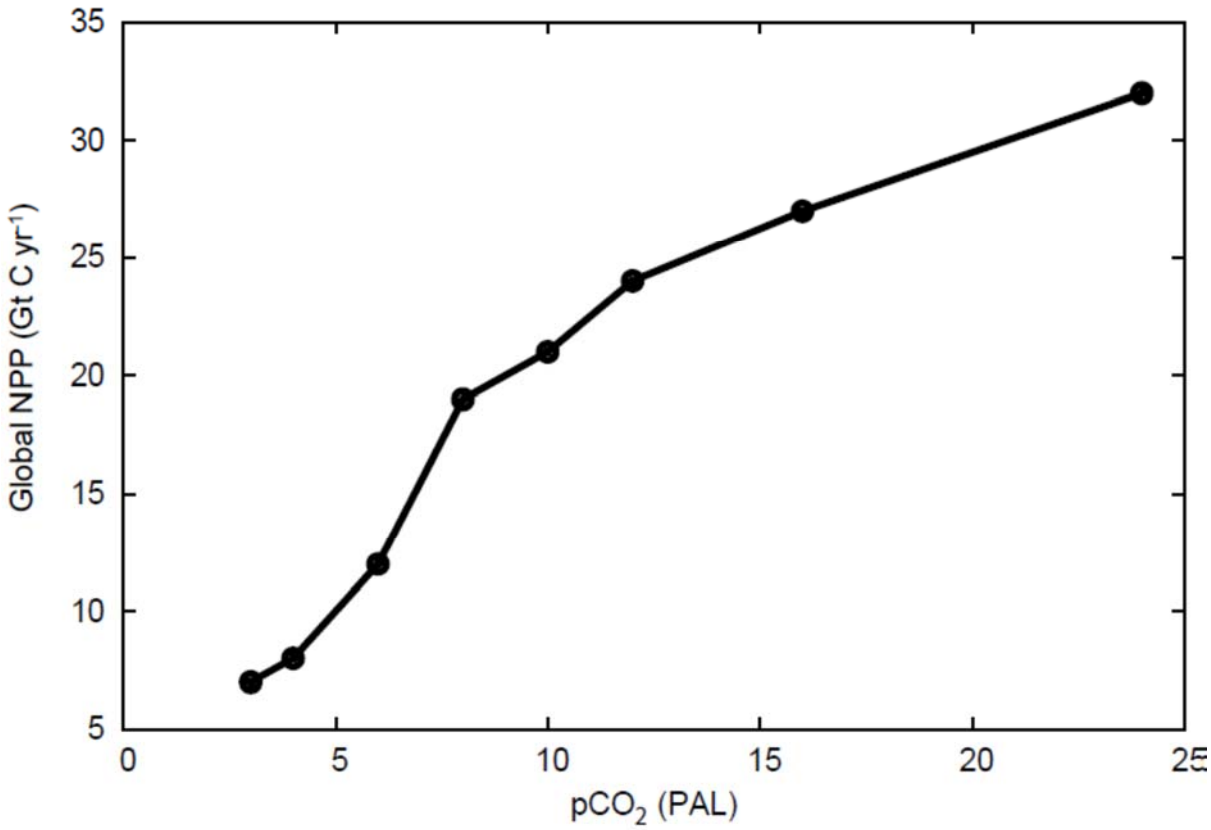

Fig. S2.

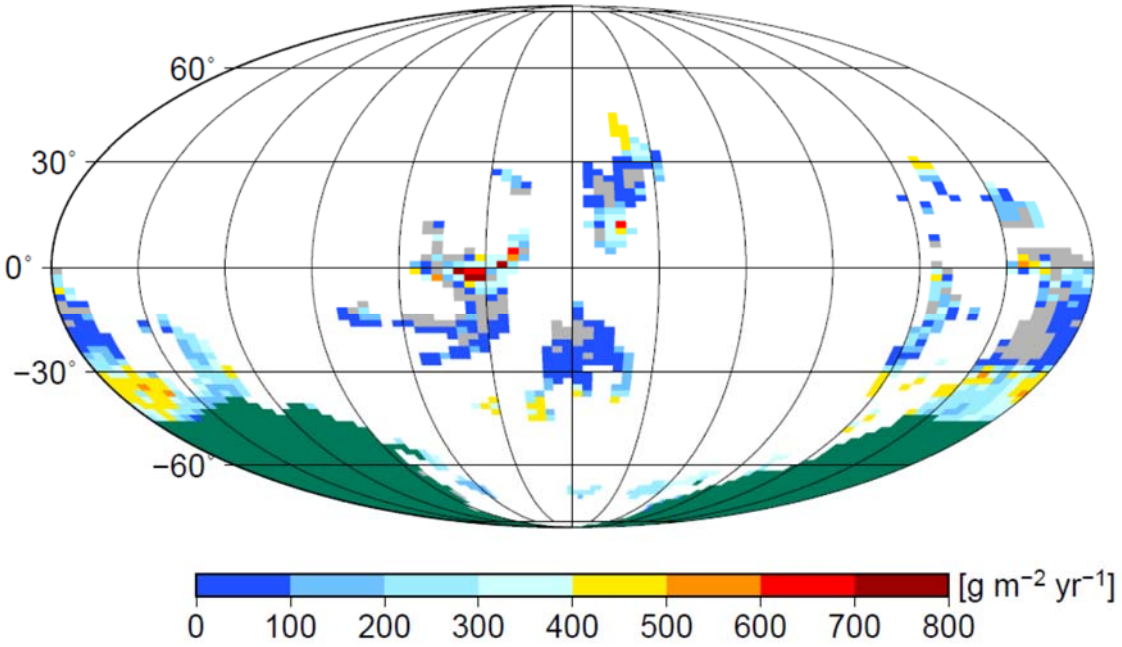

Fig. S3.

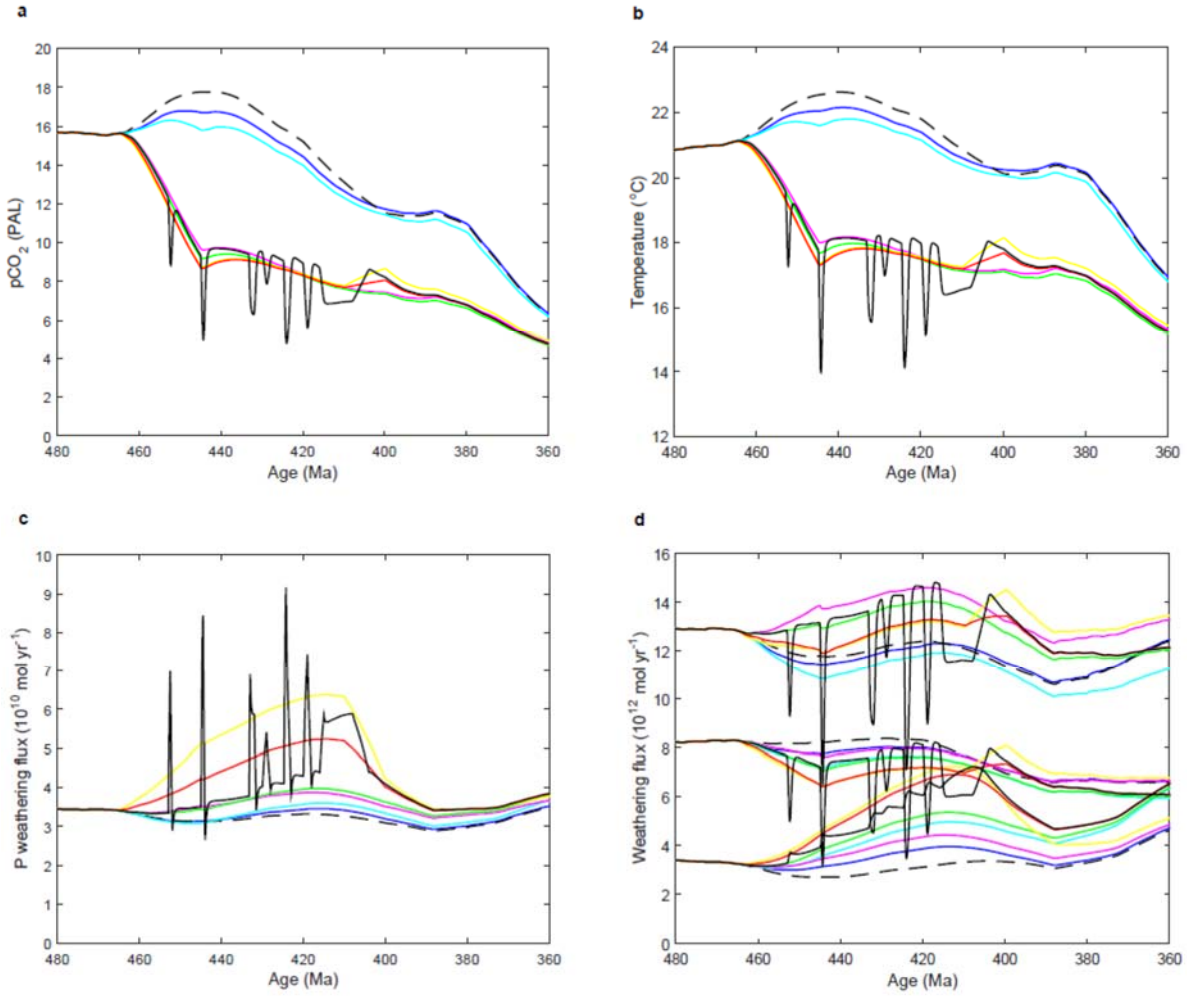
a
pCO2 (PAL)
Age (Ma)
b
Temperature (°C)
Age (Ma)
c
P weathering flux (10^10 mol yr^-1)
Age (Ma)
d
Weathering flux (10^12 mol yr^-1)
Age (Ma)

Fig. S4.

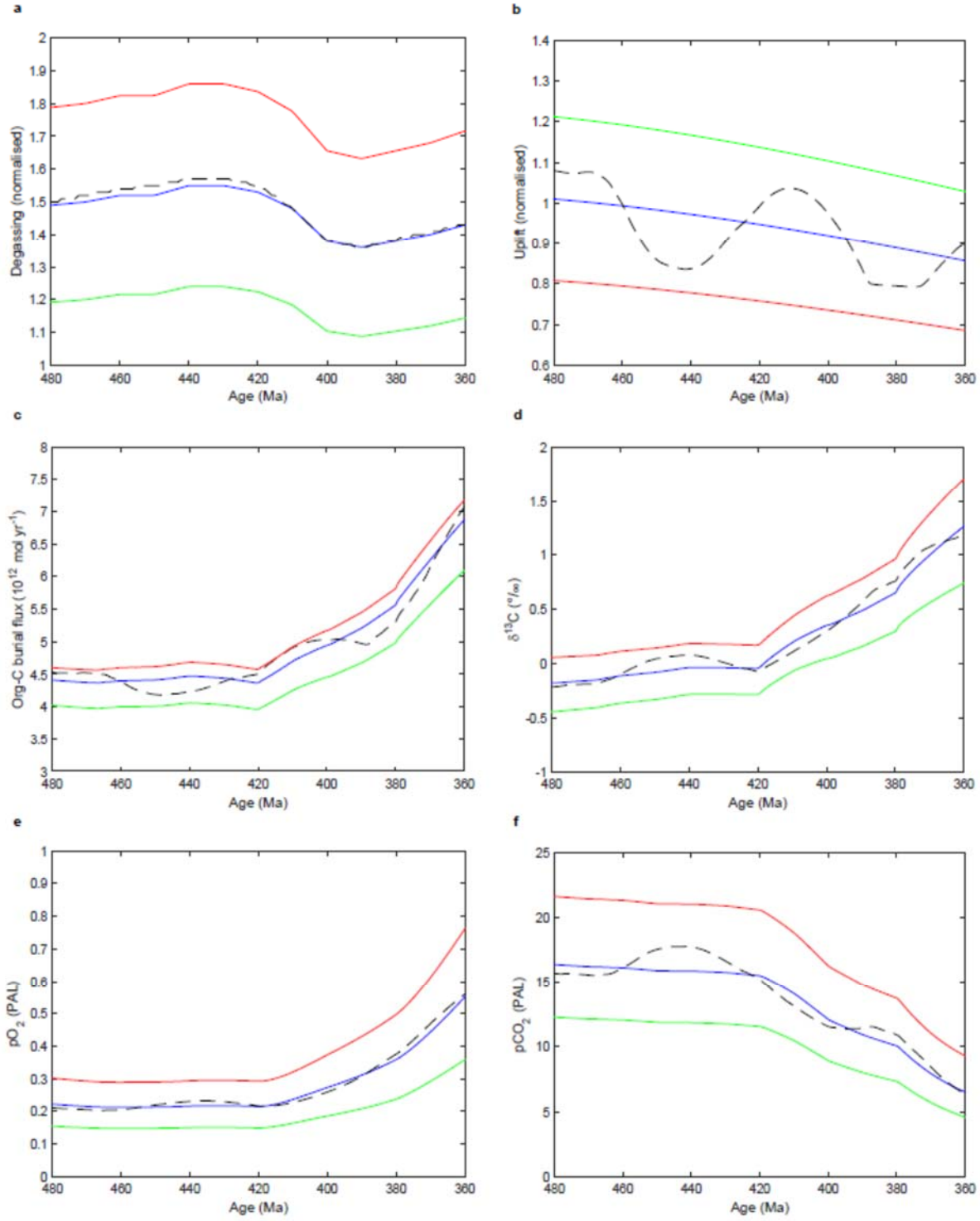
a
Degassing (normalised)
Age (Ma)
b
Uplift (normalised)
Age (Ma)
c
Org-C burial flux (10^{12} mol yr^{-1})
Age (Ma)
d
$\delta^{13}C$ (‰)
Age (Ma)
e
pO_2 (PAL)
Age (Ma)
f
pCO_2 (PAL)
Age (Ma)

Fig. S5.

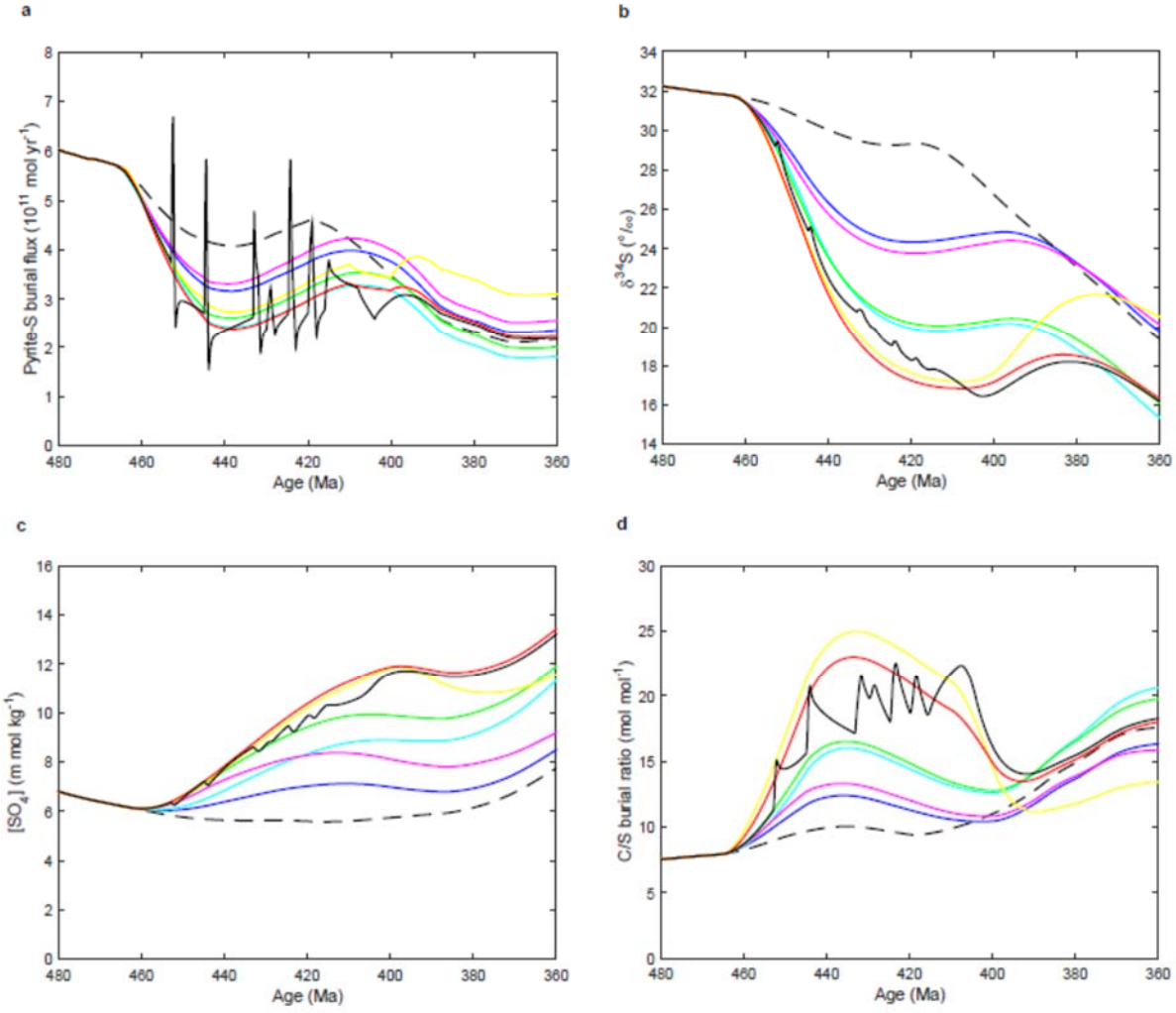
a
Pyrite-S burial flux (10^{11} mol yr^{-1})
Age (Ma)
b
$\delta^{34}S$ (‰)
Age (Ma)
c
$[SO_4]$ (m mol kg^{-1})
Age (Ma)
d
C/S burial ratio (mol mol^{-1})
Age (Ma)